PCCP

Accepted Manuscript

ROYAL SOCIETY OF CHEMISTRY

www.rsc.org/pccp

Physical Chemistry Chemical Physics

ARTICLE

High temperature oxidation of iron-iron oxide core-shell nanowires composed of iron nanoparticles

Received 00th January 20xx,
Accepted 00th January 20xx

DOI: 10.1039/x0xx00000x

www.rsc.org/

M. Krajewski,[a,*] K. Brzozka,[b] W. S. Lin,[c] H. M. Lin,[c] M. Tokarczyk,[a] J. Borysiuk,[a,d] G. Kowalski[a] and D. Wasik[a]

This work describes an oxidation process of iron-iron oxide core-shell nanowires at temperatures between 100 °C and 800 °C. Studied nanomaterial was synthesized through a simple chemical reduction of iron trichloride in an external magnetic field under a constant flow of argon. The electron microscopy investigations allowed determining that as-prepared nanowires were composed of self-assembled iron nanoparticles which were covered by 3 nm thick oxide shell and separated from each other by a thin interface layer. Both these layers exhibited the amorphous or highly-disordered characters which were traced by means of transmission electron microscopy and Mössbauer spectroscopy. The thermal oxidation was carried out under a constant flow of argon which contained the traces of oxygen. The first stage of process was related to slow transformations of amorphous Fe and amorphous iron oxides into crystalline phases and a disappearance of interfaces between iron nanoparticles forming studied nanomaterial (regime: 25 °C – 300 °C). After that, the crystalline iron core and iron oxide shell became oxidized and signals for different compositions of iron oxide sheath were observed (regime: 300 °C – 800 °C) with X-ray diffraction, Raman spectroscopy and Mössbauer spectroscopy. According to the thermal gravimetric analysis, the nanowires heated up to 800 °C under argon atmosphere gained 37% of mass in respect to their initial weight. The structure of studied nanomaterial oxidized at 800 °C was mainly composed of α-Fe_2O_3 (~ 93%). Moreover, iron nanowires treated above 600 °C lost their wire-like shapes due to their shrinkage and collapse caused by the voids coalescence.

Introduction

At present, iron nanoengineering is a rapidly developing branch of science and nanotechnology, and there is no sign of slowing down in this field. Undoubtedly, it is related to the abundance of iron in nature what favourably influences the costs of iron nanomaterials. Moreover, the simple iron compounds as iron oxides exhibit the unique optical, magnetic and surface properties. Most of them are also low toxic and biocompatible.[1] All of above mentioned features cause that iron-based nanomaterials are very promising from the viewpoint of a vast amount of biomedical applications,[2,3] energy storage devices,[4,5] catalysis systems,[6,7] magnetic devices,[8,9] etc. Other important issue of iron-based nanomaterials is that they can be easily-tailored to adequate applications. It can be achieved by changing the shapes and dimensions of nanostructures, what allows controlling their properties. Therefore, in the literature there are reported plenty of works where they take the different forms such as: nanobelts,[10] nanotubes,[11] nanoflowers,[12] and the most frequently studied nanoparticles[13-15] and nanowires.[10,15-17]

Working in the field of iron nanoengineering, researchers usually encounter on very serious problem related to a high reactivity of pure Fe. Iron exposed to air or oxygen-containing atmosphere always tends to be oxidized instantly even at room temperature. Indeed, it causes that a lot of nanomaterials take a form of so-called iron-iron oxide core-shell structures (Fe-Fe_xO_y) and they always exhibit their properties as the whole nanostructures.[18] Considering the Cabrera-Mott model of oxidation at room temperature, a rough estimation leads to conclusion that a surface of pure iron exposed to oxygen-containing atmosphere can be covered within 0.2 fs by 1 nm thick oxide layer; 40 s is needed to obtain a layer of 2 nm, 40 weeks for a layer of 3 nm, and around 600 years for a layer of 4 nm. It means that the thickness of initial oxidized layer is typically around 3 nm, what has been confirmed by the experimental results.[19,20] Such self-oxidation can be inconvenient in the case of studies on nanomaterials or

[a] Faculty of Physics, Institute of Experimental Physics, University of Warsaw, Pasteura St.5, Warsaw, 02-093, Poland.
[b] Faculty of Mechanical Engineering, Department of Physics, University of Technology and Humanities in Radom, Krasickiego St. 54, Radom, 26-600, Poland.
[c] Department of Materials Engineering, Tatung University, Taipei, 104, Taiwan, R.O.C.
[d] Institute of Physics, Polish Academy of Sciences, Al. Lotnikow 32/46, Warsaw, 02-668, Poland.
E-mail: marcin.krajewski@fuw.edu.pl; marcien1@o2.pl.

Electronic Supplementary Information (ESI) available: Information about the origin of hydrogen during iron nanowires formation and Figures S1 (EDX spectra of as-prepared iron nanowires), S2 (Elemental mapping spectra for as-prepared iron nanowires and nanowires annealed at 300 °C, 600 °C and 800 °C), S3 (XRD patterns collected between 42 ° and 48 ° for iron nanowires annealed at 500 °C, 600 °C, 700 °C and 800 °C) and S4 (all collected Mössbauer spectra). See DOI: 10.1039/x0xx00000x

nanocomposites containing metallic iron. On the other hand, the self-oxidation process has one very important advantage. It reduces greatly the rate of further oxidation and leaves the strongly adherent oxide layer which makes nanostructure stable for years at room temperature. It also has a great impact on an employment of core-shell nanostructures in the biomedical applications as well as in the soil or water remediation.[21]

The iron oxidation at high temperatures is quite well established for bulk iron (e.g. oxidation of iron substrates). The mechanism of oxidation process usually follows the parabolic law of metal oxidation.[19] According to this mechanism, the phase composition of oxide layer depends on the conditions of oxidations (temperature, oxygen pressure) as well as the distance between the oxide layer and metallic iron. In general, the structure of such oxide layer is composed of a very thick innermost wustite layer (FeO), an intermediate magnetite layer (Fe_3O_4), and a thin outermost hematite layer (α-Fe_2O_3).[21] On the other hand, the high-temperature oxidation of nanoscale iron structures is still not perfectly clear. So far, it has been proven that initially oxidized iron nanoparticles form the core-shell nanostructures rapidly even at room temperatures. Their shells are either magnetite (Fe_3O_4) or maghemite (γ-Fe_2O_3) or a mixture of them.[19,20,22] Moreover, the iron oxide shells often reveal the amorphous[18,23] or small-size polycrystalline[24] characters, what causes that it is very difficult to determine precisely the structure of this layer. After the initial oxide sheath reaches the maximum thickness (3 nm), the further oxidation can follow only if oxygen chemisorbs on this layer and at the same time thermo-emission of electrons from iron core into the oxide conduction band takes place. It leads to creation of iron ions and electrons, which are transferred outward under a strong electric field resulting from chemisorption of oxygen.[24] An increasing temperature influences the creation of higher amount of ions and electrons, which cause the thickening of oxide shell. However, changing temperature also results in the transformation of iron oxides. The phase transition of Fe_3O_4 to γ-Fe_2O_3 is possible at relatively low temperatures and it is a reason why initial oxide layer sometimes contain the mixture of these both iron oxides. The maghemite to hematite transformation has no definite transition temperature, but it has been observed in the range temperatures between 300 °C and 400 °C. Such regime of temperatures is needed due to the very different crystal structure of γ-Fe_2O_3 in respect to α-Fe_2O_3.[25,26] It is also worth noting that in the case of large nanostructures small amount of magnetite can be converted directly to hematite even at low temperatures and maghemite formation is omitted. However, the complete transition of Fe_3O_4 or mixed phase composed of Fe_3O_4 and γ-Fe_2O_3 into α-Fe_2O_3 can only occur at temperatures above 500 °C.[17,27]

The formation of voids and also the creation of hollowed nanostructures are associated with oxidation of nanoscale iron materials. In general, the vacancies are created while the iron ions diffuse outward through the initial oxide shell. Since there are many vacancies close to each other, they tend to condense in the form of void.[24] Recently, it has been reported that a critical size of iron nanoparticles exists below which they become fully-oxidized and the voids are present in their centers. Such observation is possible even at room temperature if the diameters of nanoparticles equal 8 nm or lower.[19] The oxidation of larger iron nanoparticles can lead to formation of core-shell or core-void-shell nanostructures.[24] The void layer is typically placed at the interface between iron core and oxide shell, what is related to the nanoscale Kirkendall effect which confirms that iron ions diffuse much faster through the oxide layer than oxygen ions towards the iron core.[24] Moreover, the core is linked with oxide sheath by the thin connections so-called bridges which are the fast transport paths for outward diffusion of iron ions and electrons. The bridges are usually present in the nanostructures until the source of iron coming from the core is completely run out.[28] Hence, the high temperature oxidation increases the rate of iron diffusion and can result in the formation of hollowed nanostructures.

Although a plenty of fabrication ways of iron nanostructures with different shapes are known, so far most of the reports have been published concerning the high temperature oxidation of the simplest form of nanoscale iron material – iron nanoparticles (Fe NPs), which usually take a form of iron-iron oxide core-shell nanoparticles. All of these researches have a significant impact on the present knowledge about the oxidation of iron nanomaterials. However, the question remains whether the oxidation of other iron nanostructures reveals the same character as in the case of iron nanoparticles. Hence, this work deals with the problem of the high temperature oxidation process of iron-iron oxide core-shell nanowires composed of iron nanoparticles in the slightly oxidative atmosphere. As-prepared iron nanowires (Fe NWs) have been thermally-treated at different temperatures in the range from 100 °C to 800 °C under a constant flow of argon containing the traces of oxygen. Thereby, the presented results help to understand better the possible mechanism of high temperature oxidation process of iron nanowires as well as iron nanoparticles.

Experimental section

Preparation of iron nanowires

It has been already reported that a reduction reaction of iron trichloride by sodium borohydride leads to formation of iron nanoparticles which usually tend to aggregate into the short chains.[18] Moreover, it is known that it is possible to obtain longer chains by controlling the reduction rate of Fe^{3+} ions. However, such nanowires are not perfectly straight.[29] Hence, in present studies an external magnetic field was applied to ensure that iron nanoparticles coming from the reduction reaction were aligned in lines and also the distances between them could be short enough to enable to obtain a wire-like form of iron nanostructure. Such method of iron nanowires fabrication has been successfully developed and described in the previous works.[15,17,30-32] Therefore, the detailed description of synthesis setup and the subsequent steps of iron nanowires

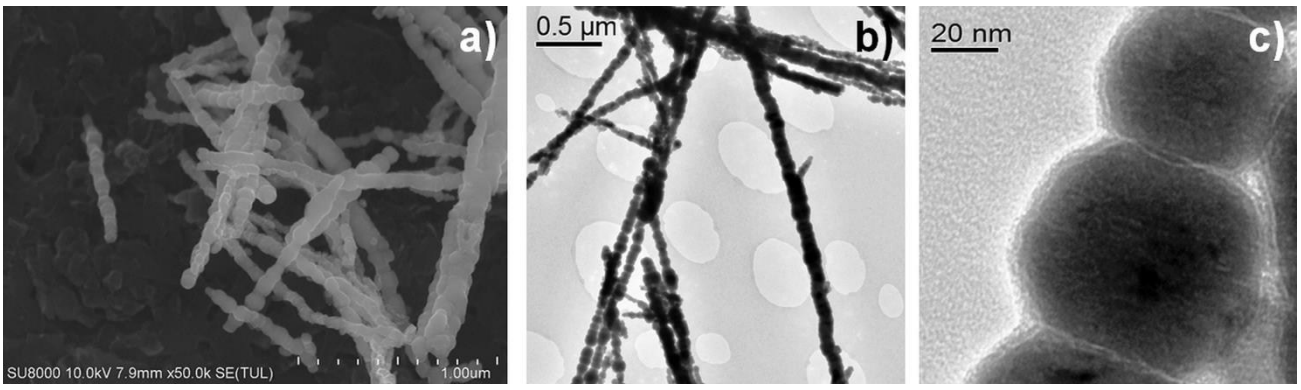

Fig. 1 a) FE-SEM and b) TEM images of as-prepared iron nanowires; c) high magnification TEM image of as-prepared single nanowire.

(Fe NWs) formation are shown in Section S1 of the Electronic Supplementary Information.

Thermal treatment of iron nanowires

The main part of this work deals with the problem of the high temperature oxidation process of iron-iron oxide core-shell nanowires. Thereby, studied nanostructure was subjected to a thermal treatment in a tube furnace (Carbolite CTF) with a constant argon flow (> 99%, Multax Company). The neutral gas atmosphere was applied during this process to decrease a spontaneous oxidation of Fe NWs by oxygen coming from air. However, it is known that iron is very reactive even with a small amount of O_2 molecules. Hence, a residual amount of oxygen presented in the applied argon and coming from the fabrication process influenced the structure and chemical composition of thermally-treated iron nanowires.[32] The high temperature oxidation process was performed via the annealing of as-prepared Fe NWs for 30 min at following temperatures: 100 °C (Fe NWs 100 °C), 200 °C (Fe NWs 200 °C), 300 °C (Fe NWs 300 °C), 400 °C (Fe NWs 400 °C), 500 °C (Fe NWs 500 °C), 600 °C (Fe NWs 600 °C), 700°C (Fe NWs 700 °C) and also at 800 °C (Fe NWs 800 °C).

Characterization

The thermal evolution of as-prepared iron nanowires was examined by means of various complementary experimental techniques, including: a Hitachi SU8020 field-emission scanning electron microscope (FE-SEM) equipped with an EMAX Evolution X-Max energy dispersive X-ray spectrometer allowing the elemental analysis and mapping, a JEOL JEM 3010 transmission electron microscope (TEM), a Phillips X'Pert diffractometer (XRD) equipped with a Cu X-ray lamp and a parallel beam Bragg reflection mirror, a T64000 Series II Raman spectrometer equipped with Nd-YAG laser (λ = 532 nm) of continuous wave excitation, a standard Mössbauer spectrometer (POLON) and ^{57}Co/Rh source of γ-radiation placed on a vibrator working in a constant acceleration mode, and a TA Instruments SDT 2960 Simultaneous DTA-TGA (TGA-DTA) equipped with an argon vessel (> 99%, Linde LienHwa Industrial Gases Co., Ltd. (Taiwan)).

Results and discussion

Two electron microscopy techniques (SEM and TEM), which enabled to study the external and internal structure of as-prepared as well as thermally-treated iron nanowires, were applied. Fig. 1 presents the typical SEM and TEM images of as-prepared Fe NWs. One can see that the obtained wire-like iron nanostructure looks like a straight chain of iron nanoparticles linked together. Additionally, each of nanoparticles is separated from the other one by a very thin interface, which is very characteristic feature of applied synthesis method. Besides that, a dark core region and a light-grey shell layer are seen. This suggests that the surface of investigated nanowires is covered by a thin oxide layer (Fig. 1c) which has been formed due to the exposition and storage of nanomaterial in the air-containing atmosphere.[15] The thickness of this layer is around 3 nm, which is consistent with the previously reported observations describing the initial oxidation of iron nanoparticles.[19,20] The presence of thin oxide layer is also confirmed by the energy dispersive X-ray (EDX) measurements of Fe NWs shown in Fig. S1 in the Electronic Supplementary Information.

The evolution of external and internal structure of as-prepared nanowires caused by thermal treatment is shown in Fig. 2 and Fig. 3. Referring to presented SEM and TEM images, as-prepared iron nanowires are composed of the spheres and each of them has its own diameter. Hence, the diameters of Fe NWs vary from 50 nm to 100 nm and their length can reach even 10 µm. However, it is worth noting that the diameters of most of nanoparticles forming investigated nanostructure are around 90 nm, while the average diameter of single nanowire can be considered as about 100 nm due to a thin iron oxide layer placed on its surface (Fig. 1c). Such nanowires have been subjected to the thermal treatment at eight temperatures ranging from 100 °C to 800 °C. The microscopic observations of their annealed forms show that the wire-like structure is maintained up to 500 °C. The annealing up to this temperature does not influence drastically the diameters and lengths of nanowires, but it causes a disappearance of the interfaces between nanoparticles forming them and also has a great impact on their roughness and the internal structural changes. The interfaces start to

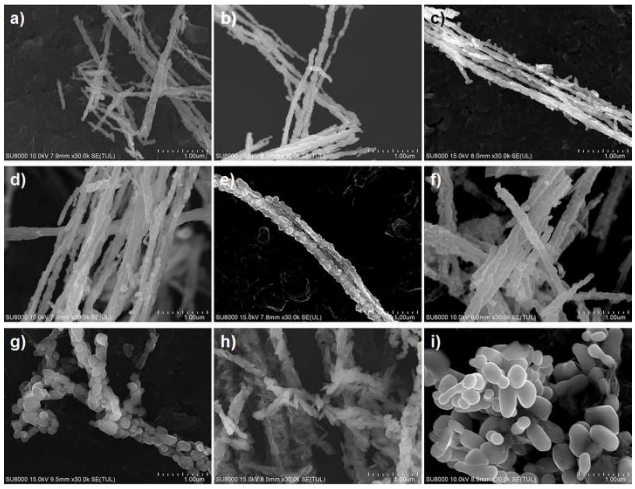

Fig. 2 SEM images of a) as-prepared and iron nanowires annealed at b) 100 °C, c) 200 °C, d) 300 °C, e) 400 °C, f) 500 °C, g) 600 °C, h) 700 °C and i) 800 °C.

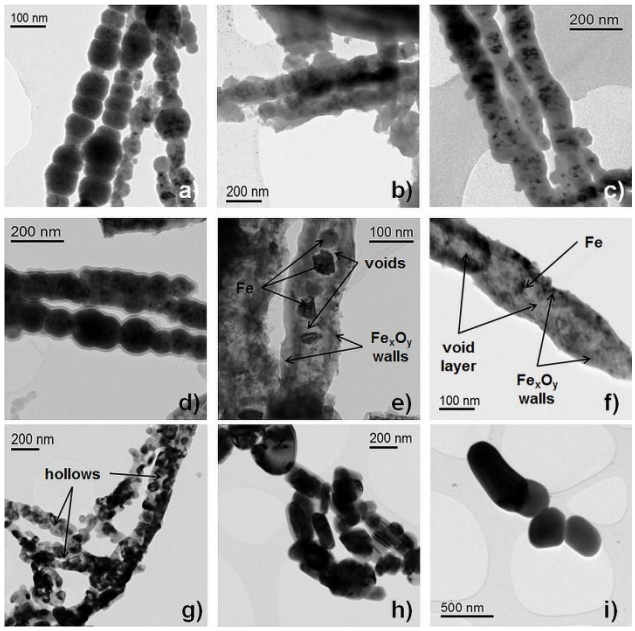

Fig. 3 TEM images of a) as-prepared and iron nanowires annealed at b) 100 °C, c) 200 °C, d) 300 °C, e) 400 °C, f) 500 °C, g) 600 °C, h) 700 °C and i) 800 °C.

vanish at quite low temperature of 100 °C, which is discussed in details later. In turn, the structural changes can be explained by the high temperature oxidation of studied nanomaterial. The elemental mapping of iron and oxygen (Fig. S2 in the Electronic Supplementary Information) collected using the EDX spectrometer indicates clearly that the signal originating from oxygen is more and more intensive with increasing annealing temperature. This is obviously related to the oxidation phenomenon. Moreover, the formation of oxide layer on the surface of studied nanomaterial accompanied the changing roughness of external nanowire walls.

The quite interesting feature of thermal treatment presented in this work is that Fe NWs lose their wire-like structure and they start forming a mixture of large microparticles and microrods at temperatures above 600 °C. However, it is commonly known that the mobility of iron ions diffusing from the bulk towards the surface is much faster at high temperatures, what increases the rate of oxidation reaction occurring rather closer to the surface than inside of nanomaterial. This induces that the surface-to-volume ratios can be changed and also it may cause a partial sticking of nanowires.[19,20,33] Moreover, the fast outward diffusion of iron ions results in the creation of vacancies which usually condense in the form of void[19,20,24] or even void layer.[24,34] Such phenomenon is easily-observed in the case of small iron nanoparticles oxidation even at relatively low temperatures (< 250 °C).[24,28] But taking into account the larger iron nanostructures, it is obvious that the higher temperatures are needed to be able to perceive the formation of voids or void layers. It has been already proven that the annealing of iron nanowires with diameters of about 55 nm at 200 °C in air is responsible for creation of voids placed at the interface between the most inner remaining non-oxidized part of iron wire and the outer oxide layer.[34] In the same reference,[34] the following heating up to 400 °C results in formation of iron oxide nanotube with a cylindrical pore and with a large number of voids situated along inner wall of the nanotube. These observations are somehow consistent with the results presented in this work. Iron nanowires annealed at 400 °C (Fig. 3e) and 500 °C (Fig. 3f) have similar structures to those from previously mentioned report which have been treated at 200 °C and at 400 °C, respectively. However, instead of cylindrical pore in the middle of nanowire for Fe NWs 500 °C, the porous layer is present which is composed of the non-oxidized residues of iron nanoparticles forming nanowire and the large number of voids crossed by iron oxide bridges which allow the fast transport of iron ions and electrons. This aspect and differences in annealing temperatures can be explained considering three following factors: size of studied nanomaterial, type of oxidizing atmosphere and also time of annealing. In this work, iron nanowires are almost twice larger than those in reference,[34] so undoubtedly higher temperatures are needed to obtain similar results of oxidation. Additionally, this study presents the thermal treatment performed not in air but in the slightly oxidizing argon atmosphere containing the residual amount of oxygen. The last important factor is related to the time of annealing. Previously published results[34] have been recorded for longer periods than 30 min i.e. 1 hour, 5 hours.

The important issue related to creation of voids during oxidation is a growth of the nanostructure size and also the formation of hallowed nanostructures which often tend to shrink and collapse at elevated temperatures.[34] Taking into account this matter, the microscopic observations of thermally-treated iron nanowires at 600 °C indicate the presence of small hollows inside them (Fig. 3g) as well as the growth of particles on the surface of nanowires which in fact break at around 700 °C. It is likely that such collapse can cause the fragmentation of Fe-Fe_xO_y nanowires into microparticles and microrods. The shapes of obtained structures depend strongly on the diameters of particles forming on nanowires and their sequences. The creation of microparticles and

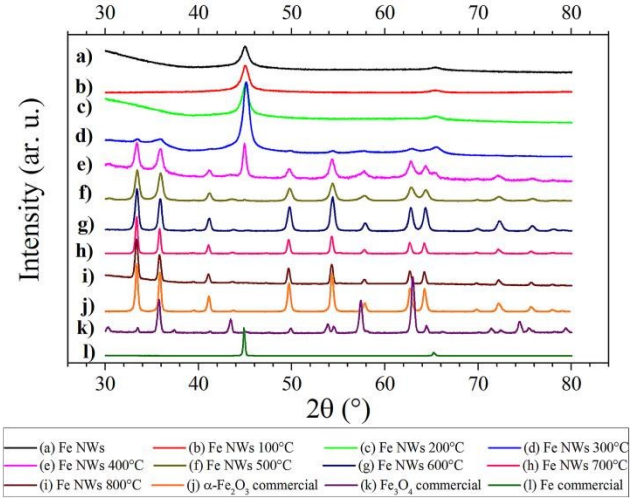

Fig. 4 XRD patterns of as-prepared iron nanowires (Fe NWs) (a) and iron nanowires annealed at 100 °C (b), 200 °C (c), 300 °C (d), 400 °C (e), 500 °C (f) and 600 °C (g), 700 °C (h) and 800 °C (i). Patters with numbers (j), (k) and (l) correspond to commercially-available equivalents of α-Fe, Fe_3O_4 and α-Fe_2O_3, respectively. The positions of peaks agree well with JCPDS cards with corresponding numbers 87–0722 (α-Fe), 87–2334 (Fe_3O_4) and 84–0311 (α-Fe_2O_3).

microrods is the result of breaking of iron nanowire in the places where the hollows inside them are large. Nevertheless, it is clearly seen that diameters of both these structures (Fe NWs 800 °C; Fig. 2i and Fig. 3i) are much larger in comparison with as-prepared nanowires (Fig. 2a and Fig. 3a). Moreover, the quite interesting feature of the thermal treatment in the slightly oxidative atmosphere is that its application allowed preventing the sintering of nanowires without their deliberate segregation during annealing process.

The powder X-ray diffraction (XRD) patterns of as-prepared as well as thermally-treated iron nanowires are demonstrated in Fig. 4. This experimental technique has enabled us to observe that indeed Fe NWs obtained during the reduction reaction of iron salt under external magnetic field are composed mainly of crystalline α-Fe phase (JCPDS card no. 87–0722). However, the broadening of the peaks indicates that studied nanomaterial can be polycrystalline with very small grains or it can contain a mixture of crystalline and amorphous iron. This is consistent with the previous observation for the short chains of iron nanoparticles produced in the reaction with usage of $NaBH_4$ as reducing agent.[18] Moreover, no signals originating from iron oxides have been detected, what proves that the oxide shell seen by electron microscopy measurements, EDX spectroscopy and elemental mapping reveals clearly amorphous character. Such structure of iron nanowires does not change significantly with increasing annealing temperature up to 300 °C. Beginning from the sample annealed at this temperature, besides the signal of crystalline iron the peaks of crystalline magnetite and hematite can be seen. The positions for both these iron oxides have been matched regarding to JCPDS database with corresponding numbers 87–2334 (Fe_3O_4) and 84–0311 (α-Fe_2O_3). In the case of Fe NWs 300 °C, the comparison of relative intensities leads to the conclusion that a predominant signal, besides the iron-related one, comes from Fe_3O_4. Therefore, it is likely that the initial iron oxide shell takes a form of an amorphous structure of Fe_3O_4, which may be caused by its partial oxidation.[22] But in the introduction section, it has been mentioned that the initial oxidation often leads to formation of a mixture of Fe_3O_4 and γ-Fe_2O_3. However, it has been already reported that in the case of iron nanoparticles the transformation of magnetite to maghemite is much faster for small nanoparticles. Thereby, the fraction of magnetite increases within the increasing size of nanoparticles.[35] Additionally, this phenomenon can be explained considering the various electrical properties of iron oxides. It is well known that the high temperature oxidation of iron leads to formation the most thermodynamically stable hematite which is a semiconductor with the bandgap between 2.1 eV and 2.2 eV.[36] However, a good conductivity of initially-formed oxide layer is needed to allow electrons passing through this layer during the further oxidation at higher temperatures. This suggests that at the beginning the relatively large iron nanostructures should be covered by magnetite with bandgap of 0.14 eV, which acts as a good conductor, rather than maghemite, which is a semiconductor with the value of bandgap close to hematite (2.03 eV).[24] XRD pattern of nanowires annealed at 300 °C also contains the signal originating from hematite. Nevertheless, it is known that for the large nanostructures a small amount of Fe_3O_4 can be converted directly to α-Fe_2O_3 even at low temperatures. In this case, the maghemite (γ-Fe_2O_3) formation is usually omitted.[17,27] Returning to XRD analysis, the oxidation of iron nanowires over 300 °C results in consumption of crystalline iron core and at the same time slow progressive transformation of Fe_3O_4 into α-Fe_2O_3. Crystalline magnetite is evidently present inside the nanostructure up to 500 °C and links the iron core with oxide shell by forming the bridges, which is consistent with previously discussed TEM observations. Nevertheless, at temperature range between 300 °C and 500 °C part of Fe_3O_4 placed closer to surface converts into hematite. The signals coming from crystalline iron are clearly visible in XRD patterns until the annealing temperature reaches about 600 °C (see Fig. S3 in the Electronic Supplementary Information) but the highest consumption of α-Fe is observed between 400 °C and 500 °C. The thermal treatment at temperatures of 700 °C and 800 °C is related to the oxidation of the residual amount of iron and magnetite, which are probably under the limit of detection of XRD. Annealing at such high temperatures aims to form the final oxidation product which indeed is α-Fe_2O_3. It is also worth noting that XRD patterns for all investigated samples have been compared with patterns for the high-purity commercial equivalents of α-Fe (99.5%, Carl Roth GmbH), Fe_3O_4 (99.99%, Sigma-Aldrich) and α-Fe_2O_3 (99.98%, Carl Roth GmbH). These measurements have been intended to facilitate the verification of peak positions for iron-containing phases in different samples.

Raman spectroscopy is a great tool to study the structural changes of growing iron oxide shell during the high temperature oxidation of iron nanowires. However, the application of this experimental technique may cause the

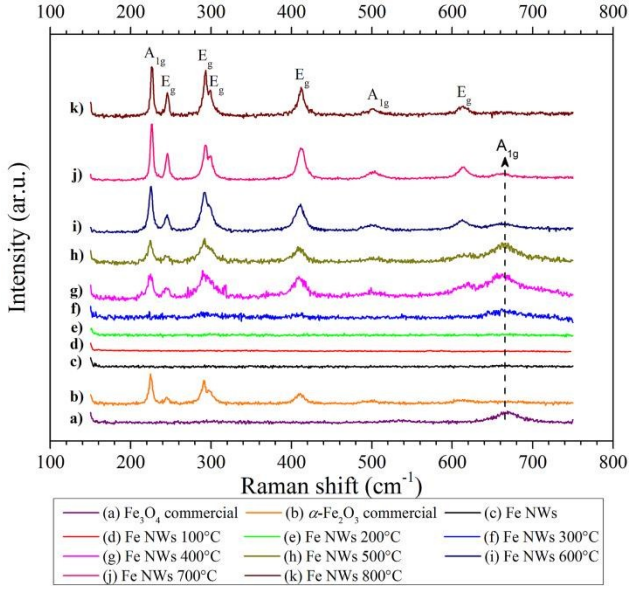

Fig. 5 Raman spectra of: commercial Fe_3O_4 (a), commercial α-Fe_2O_3 (b), as-prepared iron nanowires (Fe NWs) (c) and iron nanowires annealed at 100 °C (d), 200 °C (e), 300 °C (f), 400 °C (g), 500 °C (h) and 600 °C (i), 700 °C (j) and 800 °C (k).

irreversible heat-induced phase transitions of different iron oxide into α-Fe_2O_3 during the collecting the Raman spectrum.[37-39] Hence, in this work the low laser power of about 0.06 mW has been used to prevent such transformations. The Raman spectra of commercial powdered Fe_3O_4, commercial powdered α-Fe_2O_3 and as-prepared as well as annealed iron nanowires are shown in Fig. 5. All the spectra have been collected at room temperature in air atmosphere within 480 s using the laser with wavelength of 532 nm. The spectra recorded for commercial samples indicate that the laser power has been adjusted well to detect the signal of magnetite and hematite without any phase transformations. However, the employment of low power leads to observation only the strongest band in the spectrum of Fe_3O_4 which corresponds to position of about 668 cm^{-1} and is assigned to the A_{1g} vibrational mode.[37-39] Two other bands, which are typically located at 310 cm^{-1} (T_{2g}) and at 550 cm^{-1} (T_{2g}), have not been detected. Additionally, the spectra of commercial iron oxides are helpful for analysing more complicated plots of oxidized nanowires. Considering all the obtained spectra, it is possible to exclude the presence of γ-Fe_2O_3 which band positions and corresponding vibrational modes are typically observed at 365 cm^{-1} (T_{2g}), 511 cm^{-1} (E_g) and 700 cm^{-1} (A_{1g}).[39] Similarly to XRD results, it can be seen that Raman studies of iron nanowires thermally-treated at temperatures below 300 °C do not display any signal originating from iron oxides. This indicates that the iron oxide shell exhibits very irregular non-crystalline structure up to this temperature. Annealing at 300 °C is related to ordering the oxide structure. This enables to identify the band of magnetite located at around 668 cm^{-1} and two low-intense wide peaks at 293 cm^{-1} and 412 cm^{-1}. The origin of two weak bands can be associated with the presence of partially-oxidized magnetite[22] in the form of hematite, what has been also noticed in the case of XRD measurements. Moreover, their positions correspond well to those observed for α-Fe_2O_3. The further oxidation of iron nanowires at higher temperatures results in the formation of crystalline Fe_3O_4 and its progressive conversion to α-Fe_2O_3 phase. The presence of hematite in Raman spectra is related to observation of seven bands. Five of them with wavelength numbers 245, 293, 300, 412, and 613 cm^{-1} are assigned to the E_g vibrational modes and two remaining located at 226 cm^{-1} and 503 cm^{-1} are assigned to the A_{1g} modes.[39,40] In general, the Fe_3O_4 layer is growing on the iron nanowires only up to 400 °C and its quality seems to be practically the same at 500 °C. Comparing the bands describing magnetite and hematite, it can be seen that the initial transformation of magnetite to well-crystalline hematite begins at temperatures between 300 °C and 400 °C and almost complete conversion cannot occur below 500 °C. However, it is worth noting that there is still visible the signal coming from Fe_3O_4 at 668 cm^{-1} in the case of iron nanowires thermally-treated at 600 °C as well as at 700 °C. Such observation has been reported before and it has been attributed to either the presence of residual magnetite contamination[41,42] or the assignment of this band to the Raman forbidden (IR active) E_u mode of hematite.[39,43,44] In the case of this work, the first assumption is more reliable. This can be explained considering previously discussed XRD and TEM results. It is known that the traces of crystalline iron can be detected even for 600 °C and they are certainly connected with hematite shell by the magnetite bridges. Additionally, the complete transformation of Fe_3O_4 present inside the nanostructure may be difficult due to the application of slightly oxidizing atmosphere and the relatively thick hematite layer. According to previously described XRD results, the samples treated at 700 °C and 800 °C are composed mainly of α-Fe_2O_3 and they do not differ from each other drastically. Hence, similar Raman spectra for both of them are expected. However, iron nanowires annealed at 800 °C do not exhibit the signal of magnetite and in fact this is related to the total oxidation of studied nanomaterial. Besides that, if the band at 668 cm^{-1} represents the inactive E_u mode of iron nanowires annealed at 700 °C, it is likely that Fe NWs heated at 800 °C should also display this mode. Therefore, the assignment of this band to the Raman forbidden mode seems to be improper. Concluding this part, Raman data are indeed consistent with the electron microscopy and XRD results describing the growth of iron oxide shell and provide their supplementary information.

Structural studies performed with use of XRD and Raman spectroscopy describe well the progressive oxidation of studied nanomaterial. However, these techniques do not provide any information what happens with nanowires during the early stages of oxidation at temperatures below 300 °C. Therefore, more detailed studies characterizing the local chemical environment of iron ions in initial and annealed iron nanowires have been carried out at room temperature by means of transmission Mössbauer spectroscopy (TMS) based on ^{57}Fe isotope. The collected spectra of all samples are shown in Fig. S4 in the Electronic Supplementary Information. The identification of different iron-containing phases present in the studied samples is performed based on comparing and

Table 1. Hyperfine parameters derived for different iron-containing phases fitted to the Mössbauer spectra measured at room temperature.

Phase	IS[a)] (mm/s)	QS[b)] (mm/s)	B[c)] (T)
Crystalline α-Fe	0.00	0.00	33.05
Amorphous iron	0.03÷0.04	-0.08	24.00
Amorphous iron oxides	0.33÷0.39	0.95÷1.2	0.00
Distorted iron oxides	-0.03	-0.18	46.00÷51.00
Crystalline Fe_3O_4	0.26; 0.76	-0.03; -0.03	45.10; 48.50
Crystalline α-Fe_2O_3	0.37÷0.42	-0.15÷(-0.21)	51.30÷51.60

[a]Isomer shift in respect of pure iron. [b]Quadrupole splitting. [c]Hyperfine magnetic field (mean value).

matching the hyperfine parameters to proper phases. The values of hyperfine parameters obtained from the fits of the experimental data for spectra of Fig. S4 are collected in Table 1, while Table 2 illustrates the percentage contribution of the main components in as-prepared and thermally-treated iron nanowires. Summing up the percentage values for each row from Table 2, it is seen that most of them do not reach 100% because in fact the components with intensity below 2% are smaller than the measurement uncertainty and they have been neglected in the further analysis.

Principally, the TMS results are complementary with regard to the XRD and Raman measurements. However, this technique also delivers more information about the complexity of as-prepared nanowires and their thermally-treated derivatives; especially it enables the estimation of the quantitative share of iron atoms in the individual phases. The Mössbauer spectra, except for those obtained for as-prepared nanowires and samples annealed up to 300 °C, reveal the presence of crystalline iron oxides which quantity increases with rising annealing temperature. At the same time, it is seen that iron nanowires annealed below 300 °C are covered by two types of iron oxides which are related to the presence of amorphous and highly-distorted phases. The distorted iron oxides should be understood as the oxides which exhibit a very short range order in contrary to the completely disordered amorphous oxides. Their amounts are quite low, which is in accordance with TEM observations. Moreover, both quantity and irregularity of iron oxide shell cause that the signal coming from these oxides cannot be detected by XRD and Raman spectroscopy. The Mössbauer spectrum of initially formed nanowires indicates that in fact they contain, besides crystalline α-Fe and irregular iron oxides, a large amount of amorphous iron. According to experimental results, this amorphous phase converts into crystalline form under the influence of increasing temperature, which results in the high contribution of crystalline iron (around 40%) for nanowires annealed at temperatures up to 200 °C. However, this phenomenon starts to be inhibited above 200 °C due to the competing oxidation process. Here, it is also worth noting that the contributions of crystalline Fe and distorted iron oxides in iron nanowires thermally-treated at 100 °C shown in Table 2 comprise a bit astonishing information because the quantity of distorted iron oxides is too high with regard to other experimental results. This could be caused by too fast removal of Fe NWs from the furnace, what has influenced the rapid oxidation of newly-formed crystalline α-Fe to different distorted iron oxides. In turn, as it was noticed before, the interfaces between nanoparticles forming nanowire start to disappear at quite low temperature of 100 °C. This can be also related to the fact that they may consist of amorphous iron which becomes step by step crystalline with increasing annealing temperature. In turn, the thermal treatment of Fe NWs at 300 °C leads to formation of crystalline Fe_3O_4 as well as α-Fe_2O_3. Apart from the subspectra representing these iron oxide phases, the Mössbauer spectrum contains the signals originating from amorphous iron oxides (29%) and distorted iron oxides (9%). In contrary to XRD pattern and Raman spectrum for the same sample, the signal of crystalline magnetite is lower. Nevertheless, knowing that the initially-oxidized large iron nanostructures tend to be covered by rather magnetite than by maghemite or hematite,[35] the distorted iron oxides can be considered as a form of Fe_3O_4 with possible admixture of hematite. In such manner, part of distorted oxides can enhance the magnetite signal in the case of XRD and Raman measurements.

Table 2. Percentage contribution of the main components of Mössbauer spectra (components of intensity below 2% were omitted).

Sample	Crystalline α-Fe	Amorphous Fe	Amorphous iron oxides	Distorted iron oxides	Crystalline Fe_3O_4	Crystalline α-Fe_2O_3	Iron core interacting with hematite
Fe NWs	33	54	3	8	-	-	-
Fe NWs 100 °C	23[a)]	45	3	26[a)]	-	-	-
Fe NWs 200 °C	39	44	7	6	-	-	-
Fe NWs 300 °C	25	31	29	9	2	3	-
Fe NWs 400 °C	13	15	15	25	5	24	-
Fe NWs 500 °C	2	8	4	18	5	61	-
Fe NWs 600 °C	-	-	-	13	-	84	-
Fe NWs 700 °C	-	-	-	5	-	89	4
Fe NWs 800 °C	-	-	-	3	-	90	5

[a]After annealing of iron nanowires at 100 °C may have taken place the fast partial spontaneous oxidation reaction of crystalline iron to distorted iron oxides.

The spectrum of iron nanowires annealed at 400 °C indicates that the oxidation reaction becomes much more intensive. At this temperature the amount of crystalline and amorphous iron decreases drastically from 25% and 31% to 13% and 17%, respectively. Also, this temperature is enough to transform different iron oxides into the most thermodynamically stable hematite. On the other hand, it is insufficient for their complete conversion. Thus, the contribution of hematite starts dominating in Mössbauer spectra collected for samples annealed at temperature of 500 °C and above. Moreover, annealing at 500 °C causes the substantial drop of signal corresponding to iron and amorphous iron oxides.

The Mössbauer spectra collected for samples annealed at 600 °C, 700 °C and 800 °C prove that the oxidation finishes gradually and crystalline hematite constitutes a dominant phase of the material (84% ÷ 90%). Besides that, small traces of distorted oxides are visible (13% ÷ 3%). Moreover, another slight sextet arises and grows with increasing annealing temperature. It is characterized by a magnetic hyperfine field of about 33.8 T – 34.2 T, a quadrupole splitting of 0.18 mm/s and an isomer shift of 0.39 mm/s. A similar component has been reported in Mössbauer spectra obtained for iron nanoparticles[45] and it has been attributed to the interactions of the core iron atoms with an oxide shell of particle. Moreover, it is supposed that this sextet might be associated with iron nanoclusters which interact with hematite neighbourhood and therefore they do not show superparamagnetic relaxations.

The morphological and structural studies are supplemented with thermogravimetric analysis (TGA) combined with differential thermal analysis (DTA). The experimental data were collected simultaneously for both thermoanalytical techniques during one measurement. However, there were performed two independent TGA-DTA experiments. The first one was carried out in the slightly oxidizing argon atmosphere, while the second in the artificial air (25% oxygen and 75% nitrogen). The heating rate and the temperature range for both tests were exactly the same and equalled 5 °C per minute between 25 °C and 800 °C.

The obtained TGA-DTA curves are shown in Fig. 6. Considering only TGA spectra, it can be seen that the mass of initial sample increased significantly in both applied atmospheres. Assuming that the full oxidation of all iron present in studied nanomaterial may occur, the theoretical value of mass gain can be calculated based on Eq. 1 and equals around 43% of initial mass.[46]

$$4Fe + 3O_2 \rightarrow 2Fe_2O_3 \quad (1)$$

This assumption is in a good agreement in the case of experiment performed in the artificial air, while the annealing in argon leads to increase in weight by only 37% with regard to initial mass. Additionally, the gain of mass is much faster for iron nanowires heated in the artificial air than in the argon atmosphere. This is clearly visible at temperature region between 100 °C and 530 °C. The gain of mass slows down and reaches the level of 140% and 132% at around 530 °C and 610 °C for the artificial air and the argon atmosphere,

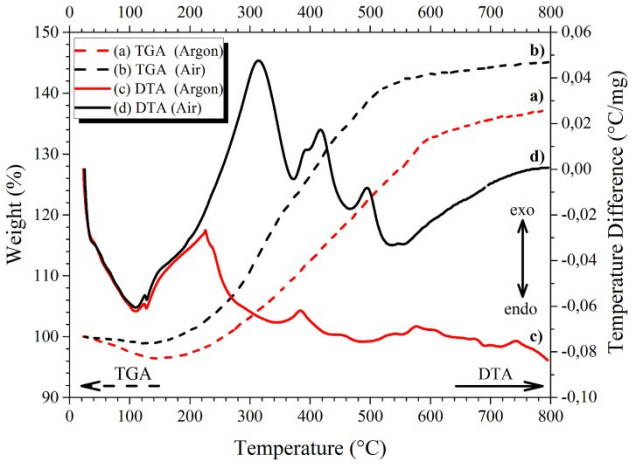

Fig. 6 TGA-DTA curves of as-prepared iron nanowires collected in the slightly oxidizing argon atmosphere (a; c) and in the artificial air (b; d).

respectively. All of these aspects indicate that the applied argon atmosphere contains a low amount of oxygen.

The previously mentioned assumption about the mass gain does not provide any information about the phase composition at different temperatures during the oxidation process but this can be done by analysing the DTA curves. Their shapes suggest a multi-step oxidation process of iron nanowires. However, the DTA spectrum collected in the argon atmosphere is quite complex to point out strictly the temperatures of each phase transition occurring in the studied nanomaterial. Therefore, the data coming from the experiment carried out in the artificial air are considered as a reference measurement. According to experimental results, both DTA curves up to 200 °C represent two endothermic processes occurring at around 100 °C and 130 °C. They are associated to the evaporation of adsorbed moisture and the partial transformation of amorphous iron into crystalline form, respectively. Moreover, the second process is perfectly confirmed by the results of Mössbauer spectroscopy. Above 200 °C, DTA curves for air and argon atmosphere differ from each other. Four exothermic peaks are clearly visible in the case of experiment performed in the artificial air. Their positions are located at around 314 °C, 394 °C, 417 °C and 495 °C and may correspond to: the oxidation of iron to amorphous or distorted iron oxides (314 °C), their partial oxidation to Fe_3O_4 as well as α-Fe_2O_3 (394 °C; 417 °C) and ultimately the formation of final product of oxidation (495 °C). Moreover, the DTA signal is endothermic in the temperature range between 510 °C and 700 °C. This suggests that the nearly fully-oxidized nanomaterial (the accordance with TGA results) is being rearranged at these temperatures. In contrary, as it has been mentioned before, the DTA spectrum recorded for the argon atmosphere is quite complicated to analyse. It is related to the fact that almost entire curve above 200 °C is under endothermic regime and the exothermic peaks referring to the oxidation are very weak. There are only three poorly distinguishable exothermic peaks located at around 385 °C, 578 °C and 741 °C. The first of them could be attributed to oxidation of iron and formation of amorphous, distorted as

well as crystalline iron oxides, the second to oxidation of Fe_3O_4 to α-Fe_2O_3, while the third to the full oxidation of residual magnetite and iron to α-Fe_2O_3. Furthermore, the phase transition at 385 °C matches perfectly to the Mössbauer spectrum of iron nanowires annealed at 400 °C. Undoubtedly, there is a stage between 385 °C and 578 °C, where the part of amorphous and distorted iron oxides transforms step by step into crystalline α-Fe_2O_3. The transformation occurring at 741 °C corresponds well to the previously discussed Raman results which show that the traces of magnetite convert to hematite between 700 °C and 800 °C. Nevertheless, the shape of DTA spectrum collected for the argon atmosphere proves that the evolution of studied nanomaterial is continuous during all annealing process. It is also worth noting that the comparison of both presented DTA curves confirms again that the applied argon atmosphere is not completely free of oxygen although its content is low. This influences the reduction of oxidation rate. For instance, the gain of mass at 300 °C observed during TGA measurements is about 3% and 11% in respect to initial mass for the argon atmosphere and the artificial air, respectively. On one hand, such temperature allows detecting the signal originating from crystalline iron oxides by XRD, Raman spectroscopy as well as TMS. On the other hand, it seems to be too low to oxidize the higher amount of iron due to the competition between iron oxidation and the crystallization of the internal amorphous phases.[47,48] Additionally, the low content of oxygen may cause the shift of phase transitions seen in the case of DTA spectrum in the argon atmosphere to higher temperatures with regard to DTA results obtained for the artificial air.

Conclusions

The results presented in this work showed that indeed iron-iron oxide core-shell nanowires composed of iron nanoparticles can be fabricated in the simple chemical reduction of iron trichloride with sodium borohydride in the external magnetic field. Such prepared nanomaterial revealed quite complex structure which consisted of highly-distorted iron oxides, amorphous iron oxides as well as amorphous iron covering crystalline iron core. This constitutes a great advantage of studied nanowires related to the enhancement of stability against the progressive oxidation in the ambient conditions. However, the main aim of this work was to study the evolution of the structure of as-prepared iron nanowires in relation to changing annealing temperature. This process was performed in the slightly oxidative argon atmosphere which was certainly contaminated by the traces of oxygen, what was confirmed by thermogravimetric analysis. This technique also allowed determining the gain of mass which reached about 37% of initial mass. Furthermore, the simultaneously collected DTA spectrum indicated that the evolution of studied nanowires was continuous during all annealing process.

According to the electron microscopy measurements, the diameters of studied nanomaterial were not uniform along the whole nanowires. This was related to the fact that nanowires were composed of iron nanoparticles with different diameters aligned in the straight line which were additionally separated from each other by a very thin interface. The progressive oxidation led to disappearance of the interfaces between nanoparticles at 100 °C, changes of surface roughness between 200 °C and 500 °C, and also internal structural changes of nanomaterial. Moreover, TEM measurements allowed observing the creation of numerous voids formed due to the fast outward diffusion of iron ions. The formation of a large number of voids resulted in the collapse and the fragmentation of iron-iron oxide core shell nanowires into microparticles and microrods at around 700 °C. Thus, the form of nanowire was not preserved during the high temperature oxidation.

The structural changes of as-prepared iron nanowires within the progressive oxidation were determined by means of XRD, Raman spectroscopy and TMS. In general, all applied techniques were complementary and showed that the contribution of iron oxides increased during the thermal treatment. The phase composition of iron nanowires depended strictly on the annealing temperature. Referring to the structural studies, in the early stages of oxidation at temperatures below 300 °C studied nanomaterial did not exhibit the well-ordered crystalline structure of iron oxides, which in fact was formed on its surface and observed in the case of TEM measurements. This caused that they could not be recognized by neither XRD nor Raman spectroscopy. On the other hand, the structural studies indicated that iron nanowires were covered by amorphous and highly-distorted iron oxides which possibly could have a form of Fe_3O_4. At temperatures between 300 °C and 700 °C, the signal originating from crystalline iron oxides was increasing gradually and was detected by all applied experimental techniques. Initially, the iron oxide shell was composed of the mixture of amorphous and highly-distorted iron oxides as well as crystalline Fe_3O_4 and α-Fe_2O_3. However, the rising temperature caused the slow transformations of iron oxides and the formation of crystalline α-Fe_2O_3 as the final oxidation product.

It is worth noting that presented experimental results indicated clearly that the applied method of synthesis had a great impact on the possible mechanism of high temperature oxidation process. The flow of inert gas during thermal treatment helped to reduce the oxidation rate of iron but the argon atmosphere did not provide a proper protection against the oxidation.

Finally, it is commonly known that the controlling of type and quantity of iron oxides situated on the surface of nanostructures is possible by understanding the oxidation mechanism of nanoscale iron materials and the establishment of their annealing conditions. These two features are very crucial from a viewpoint of future applications. Therefore, it should be underlined that the results presented in this work confirm and develop the current knowledge about the formation and the evolution of iron-iron oxide core-shell nanostructures under the influence of changing temperature.

Acknowledgements

This work was supported by the Foundation for Polish Science International PhD Projects Programme co-financed by the EU European Regional Development Fund. J.B. would like to thank the Faculty of Materials Science and Engineering of Warsaw University of Technology for using the JEOL JEM 3010 transmission electron microscope.

References

1 P. Tartaj, M. P. Morales, T. Gonzalez-Carreno, S. Veintemillas-Verdaguer and C. J. Serna, *Adv. Mater.*, 2011, **23**, 5243.
2 H. Xu, L. Cheng, C. Wang, X. X. Ma, Y. G. Li and Z. Liu, *Biomaterials*, 2011, **32**, 9364.
3 M. A. Zeeshan, S. Pane, S. K. Youn, E. Pellicer, S. Schuerle, J. Sort, S. Fusco, A. M. Lindo, H. G. Park and B. J. Nelson, *Adv. Funct. Mater.*, 2013, **23**, 823.
4 P. Poizot, S. Laruelle, S. Grugeon, L. Dupont and J. M. Tarascon, *Nature*, 2000, **407**, 496.
5 Q. T. Qu, S. B. Yang and X. L. Feng, *Adv. Mater.*, 2011, **23**, 5574.
6 H. C. Choi, S. Kundaria, D. W. Wang, A. Javey, Q. Wang, M. Rolandi and D. J. Dai, *Nano Lett.*, 2003, **3**, 157.
7 A. N. Pour, M. R. Housaindokht, S. F. Tayyari and J. Zarkesh, *J. Nat. Gas Chem.*, 2010, **19**, 284.
8 J. Tucek, R. Zboril, A. Namai and S.i. Ohkoshi, *Chem. Mater.*, 2010, **22**, 6483.
9 A. G. L. Lin, H. Y. Peng, Z. Q. Liu, T. Wu, C. L. Su, K. P. Ariando, Loh, W. Chen and A. T. S. Wee, *Small*, 2014, **10**, 1945.
10 X. G. Wen, S. H. Wang, Y. Ding, Z. L. Wang and S. H. Yang, *J. Phys. Chem. B*, 2005, **109**, 215.
11 C. J. Jia, L. D. Sun, Z. G. Yan, L. P. You, F. Luo, X. D. Han, Y. C. Pang, Z. Zhang and C. H. Yan, *Angew. Chem.-Int. Edit.*, 2005, **44**, 4328.
12 F. Q. Hu, K. W. MacRenaris, E. A. Waters, E. A. Schultz-Sikma, A. L. Eckermann and T. J. Meade, *Chem. Commun.*, 2010, **46**, 73.
13 A. K. Gupta and M. Gupta, *Biomaterials*, 2005, **26**, 3995.
14 D. L. Huber, *Small*, 2005, **1**, 482.
15 M. Krajewski, W. S. Lin, H. M. Lin, K. Brzozka, S. Lewinska, N. Nedelko, A. Slawska-Waniewska, J. Borysiuk, and D. Wasik, *Beilstein J. Nanotechnol.*, 2015, **6**, 1652.
16 Y. L. Chueh, M. W. Lai, J. Q. Liang, L. J. Chou and Z. L. Wang, *Adv. Funct. Mater.*, 2006, **16**, 2243.
17 M. Krajewski, W. S. Lin, H. M. Lin, M. Tokarczyk, S. Lewinska, N. Nedelko, A. Slawska-Waniewska, G. Kowalski, J. Borysiuk, and D. Wasik, *Phys. Status Solidi A*, 2015, **212**, 862.
18 J. T. Nurmi, P. G. Tratnyek, V. Sarathy, D. R. Baer, J. E. Amonette, K. Pecher, C. M. Wang, J. C. Linehan, D. E. Matson, R. L. Penn and M. D. Driessen, *Environ. Sci. Technol.*, 2005, **39**, 1221.
19 C. M. Wang, D. R. Baer, L. E. Thomas, J. E. Amonette, J. Antony, Y. Qiang and G. Duscher, *J. Appl. Phys.*, 2005, **98**, 094308.
20 C. M. Wang, D. R. Baer, J. E. Amonette, M. H. Engelhard, J. Antony and Y. Qiang, *J. Am. Chem. Soc.*, 2009, **131**, 8824.
21 L. Yuan, R. S. Cai, J. I. Jang, W. H. Zhu, C. Wang, Y. Q. Wang and G. W. Zhou, *Nanoscale*, 2013, **5**, 7581.
22 L. T. Kuhn, A. Bojesen, L. Timmermann, M. M. Nielsen and S. Morup, *J. Phys.-Condes. Matter*, 2002, **14**, 13551.
23 E. E. Carpenter, S. Calvin, R. M. Stroud and V. G. Harris, *Chem. Mat.*, 2003, **15**, 3245.
24 A. Cabot, V. F. Puntes, E. Shevchenko, Y. Yin, L. Balcells, M. A. Marcus, S. M. Hughes and A. P. Alivisatos, *J. Am. Chem. Soc.*, 2007, **129**, 10358.
25 P. Ayyub, M. Multani, M. Barma, V. R. Palkar and R. Vijayaraghavan, *J. Phys. C - Solid State Phys.*, 1988, **21**, 2229.
26 G. Schimanke and M. Martin, *Solid State Ion.*, 2000, **136**, 1235.
27 R. M. Cornell and U. Schwertmann, *The Iron Oxides. Structure, Properties, Reactions, Occurrences and Uses (Second ed.)*, Wiley-VCH, Weinheim, 2003.
28 S. Peng and S. Sun, *Angew. Chem.-Int. Edit.*, 2007, **46**, 1.
29 L. R. Lu, Z. H. Ai, J. P. Li, Z. Zheng, Q. Li and L. Z. Zhang, *Cryst. Growth Des.*, 2007, **7**, 459.
30 W. S. Lin, Z. J. Jian, H. M. Lin, L. C. Lai, W. A. Chiou, Y. K. Hwu, S. H. Wu, W. C. Chen and Y. D. Yao, *J. Chinese Chem. Soc.*, 2013, **60**, 85.
31 W. S. Lin, H. M. Lin, H. H. Chen, Y. K. Hwu and Y. J. Chiou, *J. Nanomater.*, 2013, 237439.
32 M. Krajewski, K. Brzozka, B. Gorka, W. S. Lin, H. M. Lin, T. Szumiata, M. Gawronski and D. Wasik, *Nukleonika*, 2015, **60**, 87.
33 A. Vesel and M. Balat-Pichelin, *Vacuum*, 2014, **100**, 71.
34 R. Nakamura, G. Matsubayashi, H. Tsuchiya, S. Fujimoto and H. Nakajima, *Acta Mater.*, 2009, **57**, 4261.
35 L. Signorini, L. Pasquini, L. Savini, R. Carboni, F. Boscherini, E. Bonetti, A. Giglia, M. Pedio, N. Mahne and S. Nannarone, *Phys. Rev. B*, 2003, **68**, 195423.
36 B. S. Zou and V. Volkov, *J. Phys. Chem. Solids*, 2000, **61**, 757.
37 O. N. Shebanova and P. Lazor, *J. Raman Spectrosc.*, 2003, **34**, 845.
38 M. Hanesch, *Geophys. J. Int.*, 2009, **177**, 941.
39 A. M. Jubb, and H. C. Allen, *ACS Appl. Mater. Interfaces*, 2010, **2**, 2804.
40 S. J. Oh, D. C. Cook, D. C. and H. E. Townsend, *Hyperfine Interact.*, 1998, **112**, 59.
41 D. L. A. de Faria, S. V. Silva and M. T. de Oliveira, *J. Raman Spectrosc.*, 1997, **28**, 873.
42 J. van der Weerda, T. Rehren, S. Firth and R. J. H. Clark, *Mater. Charact.*, 2004, **53**, 63.
43 I. V. Chernyshova, M. F. Hochella and A. S. Madden, *Phys. Chem. Chem. Phys.*, 2007, **9**, 1736.
44 Y. Y. Xu, D. Zhao, X. J. Zhang, W. T. Jin, P. Kashkarov and H. Zhang, *Physica E*, 2009, **41**, 806.
45 Y. I. Petrov and E. A. Shafranovsky, *Nucl. Instrum. Methods Phys. Res. Sect. B-Beam Interact. Mater. Atoms*, 2012, **271**, 96.
46 E. N. Lysenko, A. P. Surzhikov, S. P. Zhuravkov, V. A. Vlasov, A. V. Pustovalov and N. A. Yavorovsky, *J. Therm. Anal. Calorim.*, 2014, **115**, 1447.
47 K. S. Suslick, S. B. Choe, A. A. Cichowlas and M. W. Grinstaff, *Nature*, 1991, **353**, 414.
48 M. W. Grinstaff, M. B. Salamon and K. S. Suslick, *Phys. Rev. B*, 1993, **48**, 269.

